IEEE Access
Multidisciplinary | Rapid Review | Open Access Journal

Received June 29, 2017, accepted August 25, 2017, date of publication September 4, 2017, date of current version September 27, 2017.

Digital Object Identifier 10.1109/ACCESS.2017.2748959

ISAR Imaging With Wideband V-FM Waveforms via Dual-Channel CS-D

ZHAOYU GU[1], JIAQI LIU[2], XIAO-YI PAN[1], XIA AI[2], BENYUAN LIU[3], AND GUOYU WANG[4]

[1]State Key Laboratory of Complex Electromagnetic Environment Effects on Electronics and Information System, National University of Defense Technology, Changsha 410073, China
[2]National Key Laboratory of Science and Technology on Test Physics and Numerical Mathematics, Beijing 100000, China
[3]Department of Bio-Medical Engineering, Fourth Military Medical University, Xi'an 710032, China
[4]School of Electronic Science and Engineering, National University of Defense Technology, Changsha 410073, China

Corresponding author: Zhaoyu Gu (guzhaoyu_nudt@163.com)

This work was supported by the National Natural Science Foundation of China under Grant 61571451 and Grant 61701507.

ABSTRACT In this paper, a framework for inverse synthetic aperture radars (ISAR) imaging with wideband V-FM waveforms is investigated, where the dual-channel compressed-sensing-based dechirping (CS-D) algorithms are applied to achieve high-resolution range profiles (HRRPs) of moving targets. The final HRRPs are reconstructed via the synthesis of the two HRRPs recovered from the two independent channels with CS-D. The ISAR formation is achieved from the Fourier transform-based azimuth compression methods being applied to the rearranged 2-D array of HRRPs. Simulated trials of targets modeled as point scatterers are conducted and the final well-focused images demonstrate the effectiveness of the proposed dual-channel CS-D algorithm in ISAR imaging with wideband V-FM waveforms.

INDEX TERMS Inverse synthetic aperture radars (ISAR), V-FM waveforms, dual-channel, compressed-sensing-based dechirping (CS-D).

I. INTRODUCTION

Profiting from the wideband signals via intra-pulse or inter-pulse frequency modulation and the synthetic aperture due to the relative motion of a target and radar, modern inverse synthetic aperture radar (ISAR) can achieve high-resolution images both in the down-range and cross-range domain [1]–[3]. The signals utilized in modern imaging radars are usually called large time and band product signals, such as the chirp, and frequency-stepped signals [4]–[9]. The radar detecting range can be improved by increasing the time duration while high range resolution can be achieved by pulse compression techniques. Chirp signals are one of most common large time and band product signals and have an advantage of being non-sensitive to Doppler shift in the returned radar signals. The pulse compression of chirp signals usually is accomplished using a matching filter (MF). However, due to the special characteristics of chirp signals and the small imaging scene of ISAR, the dechirping method can also finish the pulse compression, which intrinsically uilizes a long processing time to reduce the sampling rate. Scattering centers of targets in different down-range bins can be distinguished from each other when using a lower sampling rate via dechirping in contrast to using MF-based methods, where the wideband waveforms are mixed with a reference signal with the same chirp rate as the transmitted chirp signal [10], [11]. After the dechirping process, signals from the scattering centers in different down-range bins are referred to corresponding single frequencies and can be resolved by a Fourier transform (FT). However, inevitable ambiguity appears in the range and velocity when chirp signals are utilized since the ambiguity function of chirp signals is the ''ridge'' type.

Due to the ''thumbtack'' ambiguity function as depicted in reference [12], V-FM signals can mitigate the ambiguity that appear in range and velocity while achieving high resolution range profiles (HRRPs). V-FM signals can be seen as the synthesis of two chirp signals with opposite slopes; thus, the pulse compression can be achieved by a dual-channel MF. A signal can be recovered exactly from samples uniformly sampled by an analog-to-digital converter (ADC) whose sampling frequency must be at least twice that of the maximum frequency of the signal, according to the Nyquist sampling theorem. Thus, a high-speed ADC is essential to reconstruct the wideband V-FM signals, which may become practically infeasible. How to reduce the sampling rate or cut down the number of samples in V-FM waveforms is an open question that this paper seeks to address.

Recently, there has been a growing interest in reconstructing unknown sparse signals from very limited samples via compressed sensing (CS) [13]–[15]. Instead of observing

the entire signals in all coordinates, reconstruction of signals expressed in the sparse bases can be achieved by solving an optimization problem with a high probability. For radar imaging, the advantages of CS are primarily associated with the capability of obtaining high-resolution images from a limited number of measurements thus reducing the amount of data to be stored and processed [6], [16]–[20]. Dual-channel dechirping methods used to accomplish pulse compression of V-FM signals are addressed first. Then, inspired by CS and dual-channel dechirping, HRRPs of V-FM waveforms are reconstructed using the dual-channel CS-based dechirping (CS-D) method. The novelty of this paper is that the pulse compression of V-FM waveforms is achieved by the proposed dual-channel CS-D and the potential of V-FM waveforms in ISAR imaging is also validated.

The rest of the paper is organized as follows. The signal model of V-FM waveforms and pulse compression via dual-channel dechirping are explored in Section II. In section III, pulse compression of V-FM waveforms via the proposed dalchannel CS-D is addressed in detail and simulation trials are conducted in Section IV to demonstrate the effectiveness of the method. Finally, the most relevant conclusions are given in Section V.

II. SIGNAL MODEL OF V-FM WAVEFORMS

The signal model of V-FM waveforms and the corresponding HRRPs reconstruction via dual-channel dechirping are investigated in the following.

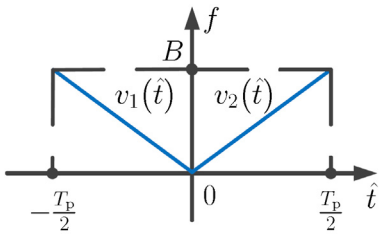

FIGURE 1. Sketch map of V-FM waveforms.

A. SIGNAL MODELING OF V-FM ECHOES

As shown in Fig. 1, suppose that the V-FM waveforms are composed of two chirp signals with opposite slopes and can be expressed as

$$v\left(\hat{t}\right) = \mathrm{rect}^{-}_{\mathrm{half}}\left(\frac{\hat{t}}{T_{\mathbf{P}}}\right) v_1\left(\hat{t}\right) + \mathrm{rect}^{+}_{\mathrm{half}}\left(\frac{\hat{t}}{T_{\mathbf{P}}}\right) v_2\left(\hat{t}\right) \quad (1)$$

where

$$\mathrm{rect}^{-}_{\mathrm{half}}\left(\frac{\hat{t}}{T_P}\right) = \begin{cases} 1 & \hat{t} \in \left[-\frac{T_P}{2}, 0\right] \\ 0 & \text{else} \end{cases}$$
$$\mathrm{rect}^{+}_{\mathrm{half}}\left(\frac{\hat{t}}{T_P}\right) = \begin{cases} 1 & \hat{t} \in \left[0, \frac{T_P}{2}\right] \\ 0 & \text{else} \end{cases} \quad (2)$$

$$v_1\left(\hat{t}\right) = \begin{cases} \exp\left(-j\pi\gamma\hat{t}^2\right) & \hat{t} \in [-\infty, 0] \\ 0 & \hat{t} \in (0, +\infty] \end{cases}$$
$$v_1\left(\hat{t}\right) = \begin{cases} 0 & \hat{t} \in [-\infty, 0] \\ \exp\left(j\pi\gamma\hat{t}^2\right) & \hat{t} \in (0, +\infty] \end{cases} \quad (3)$$

γ is the chirp rate, T_P is the pulse width and $\hat{t}$ represents the fast time.

The transmitted V-FM waveform can be expressed as follows

$$\begin{aligned} s\left(\hat{t}, t_m\right) &= v\left(\hat{t}\right) \exp\left(j2\pi f_0 t\right) \\ &= \mathrm{rect}^{-}_{\mathrm{half}}\left(\frac{\hat{t}}{T_P}\right) \exp\left(j2\pi\left(f_0 t - \frac{1}{2}\gamma\hat{t}^2\right)\right) \\ &\quad + \mathrm{rect}^{+}_{\mathrm{half}}\left(\frac{\hat{t}}{T_P}\right) \exp\left(j2\pi\left(f_0 t + \frac{1}{2}\gamma\hat{t}^2\right)\right) \end{aligned} \quad (4)$$

where f_0 is the frequency of carrier wave, t_m is the slow time, t is the full time and $\hat{t} = t - t_m$. Suppose that the pulse repetition interval (PRI) of radar is $T_{\mathbf{PRI}}$, then $t_m = mT_{\mathbf{PRI}}$.

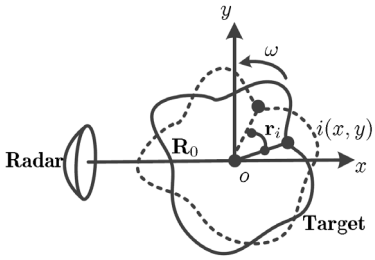

FIGURE 2. Geometry of ISAR imaging.

Without loss of generality, the local coordinate system xoy is on the moving target and the point o of the moving target is chosen as the origin, as seen in the ISAR imaging model in Fig. 2. The radar line of sight (LOS) is set as the x axis. The moving target has the circular motion with a rotation rate of ω rad/s and the vector from ISAR to o is denoted as $\mathbf{R}_0$.

Consider a scattering center $i\,(x, y)$ on the moving target with $\sigma_{\mathbf{i}}$ as the scattering coefficient. Assume that the target is at the far field of the radar and modeled as if it contains K strongest scattering centers, the echo of the scattering center i can be written as

$$\begin{aligned} &s_r\left(\hat{t}, t_m\right) \\ &= \sum_{i=1}^{K} \sigma_i s\left(\hat{t} - \frac{2\left|\mathbf{R}_i\right|}{c}, t_m\right) \\ &= \sum_{i=1}^{K} \sigma_i \mathrm{rect}^{-}_{\mathrm{half}}\left(\frac{\hat{t} - \frac{2|\mathbf{R}_i|}{c}}{T_p}\right) \\ &\quad \times \exp\left(j2\pi\left(f_0\left(t - \frac{2\left|\mathbf{R}_i\right|}{c}\right) - \frac{1}{2}\gamma\left(\hat{t} - \frac{2\left|\mathbf{R}_i\right|}{c}\right)^2\right)\right) \end{aligned}$$

$$+\sum_{i=1}^{K}\sigma_i \mathrm{rect}_{\mathrm{half}}^{+}\left(\frac{\hat{t}-\frac{2|\mathbf{R}_i|}{c}}{T_p}\right)\times\exp\left(j2\pi\left(f_0\left(t-\frac{2|\mathbf{R}_i|}{c}\right)-\frac{1}{2}\gamma\left(\hat{t}-\frac{2|\mathbf{R}_i|}{c}\right)^2\right)\right) \tag{5}$$

where $|\cdot|$ is the Euclidean norm, $\mathbf{R}_i=\mathbf{R}_0+\mathbf{r}_i$ is the vector from ISAR to the scattering center i, $\mathbf{r}_i$ is the vector from o to the scattering center i and c is the speed of the electromagnetic wave.

B. PULSE COMPRESSION VIA DUAL-CHANNEL DECHIRPING

The reference signals of the two channels can be expressed respectively as

$$s_{ref-1}\left(\hat{t},t_m\right)=\mathrm{rect}_{\mathrm{half}}^{-}\left(\frac{\hat{t}-\frac{2R_{ref}}{c}}{T_{ref}}\right)\times\exp\left(j2\pi\left(f_0\left(t-T_{ref}\right)-\frac{1}{2}\gamma\left(\hat{t}-T_{ref}\right)^2\right)\right) \tag{6}$$

$$s_{ref-2}\left(\hat{t},t_m\right)=\mathrm{rect}_{\mathrm{half}}^{+}\left(\frac{\hat{t}-\frac{2R_{ref}}{c}}{T_{ref}}\right)\times\exp\left(j2\pi\left(f_0\left(t-T_{ref}\right)+\frac{1}{2}\gamma\left(\hat{t}-T_{ref}\right)^2\right)\right) \tag{7}$$

where $R_{\mathbf{ref}}$ is the reference range, $T_{\mathbf{ref}}$ is the reference pulse duration and $T_{\mathbf{ref}}=2R_{\mathbf{ref}}/c$.

The time-domain compressed signals of the two channels after dechirping are given as follows

$$s_{\text{if-1}}\left(\hat{t},t_m\right)=\sum_{i=1}^{K}\sigma_i\mathrm{rect}_{\mathrm{half}}^{-}\left(\frac{\hat{t}-\frac{2R_i}{c}}{T_P}\right)\exp\left(\frac{j4\pi\gamma}{c}\left(\hat{t}-\frac{2R_{ref}}{c}\right)R_\Delta\right)\times\exp\left(-\frac{j4\pi\gamma}{c^2}R_\Delta^2\right)\exp\left(-\frac{j4\pi f_0R_\Delta}{c}\right) \tag{8}$$

$$s_{\text{if-2}}\left(\hat{t},t_m\right)=\sum_{i=1}^{K}\sigma_i\mathrm{rect}_{\mathrm{half}}^{+}\left(\frac{\hat{t}-\frac{2R_i}{c}}{T_P}\right)\exp\left(\frac{j4\pi\gamma}{c}\left(\frac{2R_{ref}}{c}-\hat{t}\right)R_\Delta\right)\times\exp\left(\frac{j4\pi\gamma}{c^2}R_\Delta^2\right)\exp\left(-\frac{j4\pi f_0R_\Delta}{c}\right) \tag{9}$$

where $R_\Delta=|\mathbf{R}_i|-R_{\mathbf{ref}}$.

The first exponentials of $s_{\mathbf{if-1}}\left(\hat{t},t_m\right)$ and $s_{\mathbf{if-2}}\left(\hat{t},t_m\right)$ in (8) and (9) are the range items which produce beat frequencies $2\gamma R_{\mathbf{\Delta}}/c$ and $-2\gamma R_{\mathbf{\Delta}}/c$, respectively. The second exponentials of $s_{\mathbf{if-1}}\left(\hat{t},t_m\right)$ and $s_{\mathbf{if-2}}\left(\hat{t},t_m\right)$ in (8) and (9) are the residual video phases (RVPs) and the third exponentials account for Doppler shift. After taking the FT of (8) and (9) in terms of t and multiplying by a constant conversion coefficient $2\gamma/c$, the corresponding HRRPs of the two channels in the down-range domain are obtained as follows

$$S_{\text{if-1}}\left(r,t_m\right)=\sum_{i=1}^{K}\frac{T_P\sigma_i}{2}\sin c\left(\frac{\gamma T_P}{c}\left(r-R_\Delta\right)\right)\times\exp\left(-j\frac{4\pi\gamma}{c^2}R_\Delta^2\right)\exp\left(-j\frac{4\pi f_0R_\Delta}{c}\right) \tag{10}$$

$$S_{\text{if-2}}\left(r,t_m\right)=\sum_{i=1}^{K}\frac{T_P\sigma_i}{2}\sin c\left(\frac{\gamma T_P}{c}\left(r+R_\Delta\right)\right)\times\exp\left(j\frac{4\pi\gamma}{c^2}R_\Delta^2\right)\exp\left(-j\frac{4\pi f_0R_\Delta}{c}\right) \tag{11}$$

where r represents the down-range domain.

It can be seen that the two HRRPs from the dual-channel dechirping have the same amplitude but are symmetrical about zero in the down-range domain. After the two HRRPs are achieved and the RVPs are removed, the final synthesized HRRPs can be obtained as

$$\begin{aligned}S_{if}\left(r,t_m\right)&=S_{\text{if-1}}\left(r,t_m\right)+fliplr_r\left(S_{\text{if-2}}\left(r,t_m\right)\right)\\&=\sum_{i=1}^{K}T_P\sigma_i\sin c\left(\frac{\gamma T_P}{c}\left(r-R_\Delta\right)\right)\times\exp\left(-j\frac{4\pi f_0R_\Delta}{c}\right)\end{aligned} \tag{12}$$

where $fliplr_r\left(\bullet\right)$ represents flipping the left part of the HRRPs to the right part.

From (10), (11) and (12), it can be concluded that before the final synthesized HRRPs can be achieved, the RVPs of HRRPs of each channel should first be removed.

III. PULSE COMPRESSION VIA DUAL-CHANNEL CS-D

Only considering the peak values of the HRRPs from the two channels, the derivation of (10) and (11) can be rewritten as

$$S_{\text{if-1}}\left(r,t_m\right)=\sum_{i=1}^{K}a_i\delta\left(\frac{\gamma T_P}{c}\left(r-R_\Delta\right)\times\exp\left(-j\frac{4\pi\gamma}{c^2}R_\Delta^2\right)\right) \tag{13}$$

and

$$S_{\text{if-2}}\left(r,t_m\right)=\sum_{i=1}^{K}a_i\delta\left(\frac{\gamma T_P}{c}\left(r+R_\Delta\right)\times\exp\left(j\frac{4\pi\gamma}{c^2}R_\Delta^2\right)\right) \tag{14}$$

where $a_i=T_P\sigma_i/2\exp\left(-j4\pi f_0R_{\mathbf{\Delta}}/c\right)$ and $\delta\left(\bullet\right)$ is the delta function. From (13) and (14), it can be seen that the two HRRPs are sparse since there are only a few peak values with a nonzero amplitude. The sparsity of the two HRRPs via the dual-channel dechirping paves a way for pulse compression via CS-D as addressed in the following.

Assume that the ISAR imaging region along the down-range is from r_0 to r_1 which means that $R_\Delta\in[r_0,r_1]$ and

ρ_r is the down-range resolution, then the number of range bins can be calculated as $Q = (r_1 - r_0)/\rho_r$. The dense dictionary of CS-D of the two channels can be constructed as

$$\begin{aligned} \mathbf{a}^T &= \left[a_1, a_2, \ldots, a_q, \ldots, a_Q\right]_{1\times Q} \\ a_q &= \frac{T_q \sigma_q}{2} \exp\left(-j\frac{4\pi f_0 \Delta r_q}{c}\right) \end{aligned} \tag{15}$$

where σ_q is the backscattering coefficient of the q-th range bin (i.e., Δr_q) and $\Delta r_q = r_0 + q\rho_r$, $q \in [0, Q-1]$. If there is no scattering center in the q-th range bin, then $\sigma_q = 0$ (i.e., $a_q = 0$). Taking noise into account, (8) can be cast into the CS-D framework as

$$\mathbf{s}_{\text{if-1}} = \text{IFT}\left[S_{\text{if-1}}\right] = \text{IFT}\left[\mathbf{\Theta}_1\right] + \mathbf{n} = \mathbf{\Psi}\mathbf{\Theta}_1 + \mathbf{n} \tag{16}$$

where

$$\mathbf{\Psi} = \text{IFT}\left[\mathbf{I}_{Q\times Q}\right] \tag{17}$$

is the IFT sparse basis matrix ($Q \times Q$ identity matrix)

$$\begin{aligned} \mathbf{\Theta}_1^T = \Bigg[& a_1 \exp\left(-j\frac{4\pi\gamma r_0^2}{c^2}\right), \\ & a_2 \exp\left(-j\frac{4\pi\gamma (r_0+\rho_r)^2}{c^2}\right), \ldots, \\ & a_q \exp\left(-j\frac{4\pi\gamma (r_0+q\rho_r)^2}{c^2}\right), \ldots, \\ & a_Q \exp\left(-j\frac{4\pi\gamma r_1^2}{c^2}\right)\Bigg]_{1\times Q} \end{aligned} \tag{18}$$

is the $1\times Q$ sparse weighting coefficient vector of channel one with K ($K \ll Q$) nonzero elements and largest coefficients undergoing a power decay law, which is also the recovered HRRPs via CS-D range compression and $\mathbf{n}$ is the additive complex white Gaussian noise.

Similarly, (9) can be cast into the CS framework as

$$\mathbf{s}_{\text{if-2}} = \text{IFT}\left[S_{\text{if-2}}\right] = \text{IFT}\left[\mathbf{\Theta}_2\right] + \mathbf{n} = \mathbf{\Psi}\mathbf{\Theta}_2 + \mathbf{n} \tag{19}$$

where

$$\begin{aligned} \mathbf{\Theta}_2^T = \Bigg[& a_1 \exp\left(j\frac{4\pi\gamma r_0^2}{c^2}\right), a_2 \exp\left(j\frac{4\pi\gamma (r_0+\rho_r)^2}{c^2}\right), \ldots, \\ & a_q \exp\left(j\frac{4\pi\gamma (r_0+q\rho_r)^2}{c^2}\right), \ldots, \\ & a_Q \exp\left(j\frac{4\pi\gamma r_1^2}{c^2}\right)\Bigg]_{1\times Q} \end{aligned} \tag{20}$$

is the $1 \times Q$ sparse weighting coefficient vector of channel two.

Thus, $\mathbf{s}_{\text{if}-1}$ and $\mathbf{\Theta}_1$, and $\mathbf{s}_{\text{if}-2}$ and $\mathbf{\Theta}_2$ are equivalent representations of the same signals, with $\mathbf{s}_{\text{if}-1}$ and $\mathbf{s}_{\text{if}-2}$ in the original domainčand $\mathbf{\Theta}_1$ and $\mathbf{\Theta}_2$ in the $\mathbf{\Psi}$ domain. Under certain sufficient conditions, the sparse solution to the linear inverse problem can be uniquely determined via the following convex optimization problem

$$\begin{aligned} &\min\left(\|\mathbf{\Theta}_1\|_1\right), \quad \text{s.t. } \|\mathbf{\Phi}\mathbf{s}_{\text{if-1}} - \mathbf{\Phi}\mathbf{\Psi}\mathbf{\Theta}_1\|_2 \le \varepsilon \\ &\min\left(\|\mathbf{\Theta}_2\|_1\right), \quad \text{s.t. } \|\mathbf{\Phi}\mathbf{s}_{\text{if-2}} - \mathbf{\Phi}\mathbf{\Psi}\mathbf{\Theta}_2\|_2 \le \varepsilon \end{aligned} \tag{21}$$

where **min** $(\bullet)$ is the minimization, $\|\bullet\|_p$ is the ℓ_p norm, $\mathbf{\Phi}$ is the measurement matrix with $M \times Q$ elements, and ε is the noise level.

Since the range compression via CS with far fewer measurements means that $M < Q$, the recovery of $\mathbf{\Theta}_1$ from the measurements $\mathbf{\Phi}\mathbf{s}_{\text{if}-1}$ and the recovery of $\mathbf{\Theta}_2$ from the measurements $\mathbf{\Phi}\mathbf{s}_{\text{if}-2}$ are usually unsuccessful. Thanks to $\mathbf{\Theta}_1$ and $\mathbf{\Theta}_2$ being sparse with K nonzero elements or the largest coefficients, when the matrix $\mathbf{\Phi}\mathbf{\Psi}$ has the restricted isometry property (RIP), it is probable that one is able to reconstruct the K nonzero elements or largest coefficients from a similarly sized set of $M = O(K\mathbf{log}(Q))$ measurements $\mathbf{\Phi}\mathbf{s}_{\text{if}-1}$ and $\mathbf{\Phi}\mathbf{s}_{\text{if}-2}$ by solving a convex ℓ_1 optimization problem. Then, the finally reconstructed HRRPs can be obtained by the sum of $\mathbf{\Theta}_1$ and $\mathbf{\Theta}_2$ after each of the RVPs are removed, which can be represented as

$$\mathbf{\Theta}^T = \left[\mathbf{\Theta}_1^* + \mathbf{\Theta}_2^*\right] = 2\left[a_1, a_2, \ldots, a_q, \ldots, a_Q\right]_{1\times Q} \tag{22}$$

where $\mathbf{\Theta}_1^*$ and $\mathbf{\Theta}_2^*$ represent $\mathbf{\Theta}_1$ and $\mathbf{\Theta}_2$, respectively, after the RVPs are removed.

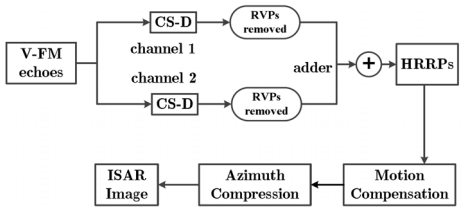

FIGURE 3. Flow chart of ISAR imaging with wideband V-FM waveforms via dual-channel CS-D.

After the HRRPs are reconstructed from the dual-channel CS-D and rearranged in to a two-dimensional (2D) array, the motion compensation methods (such as envelope correlation) and the azimuth compression algorithms (such as FT) can be applied on the 2D array to achieve the final ISAR image. The flow chart of HRRPs reconstruction and ISAR image formation with wideband V-FM waveforms via dual-channel CS-D are shown in Fig. 3.

IV. SIMULATIONS

To verify the performance of dual-channel CS-D in V-FM ISAR imaging, targets modeled as point scatterers are utilized in the following, as shown in Fig. 4. The V-FM ISAR works at the X-band with a carrier frequency of 10 GHz and bandwidth of 300 MHz. The pulse-width is 100 μs and the pulse repetition frequency is 1 kHz. The number of down-range samples of each channel is 32, thus the total number of down-range samples is 64 (selected evenly) , which is significantly fewer than that of conventional pulse compression algorithms under the Nyquist sampling theorem, such as MF.

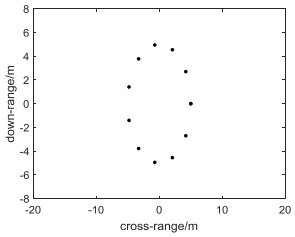

FIGURE 4. The point scatterers modeling of target.

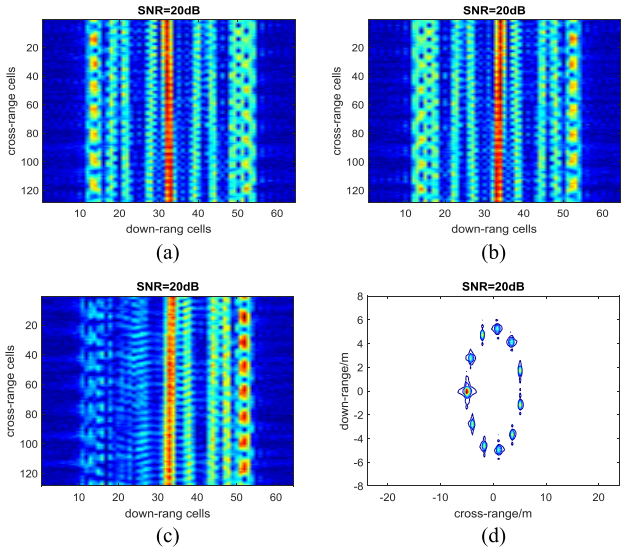

FIGURE 5. Pulse compression and ISAR imaging via dual-channel dechirping. (a) HRRPs of channel 1. (b) HRRPs of channel 2. (c) Synthesized HRRPs. (d) ISAR imaging.

A. PULSE COMPRESSION VIA DUAL-CHANNEL DECHIRPING AND DUAL-CHANNEL CS-D

In total, 128 pulses with a time duration of T_M =0.128 s are transmitted and collected to yield the 2D ISAR image formation. The signal-to-noise ratio (SNR) is set to be 20 dB. The pulse compression signals of channel one and channel two after motion compensation are shown in Fig. 5(a) and Fig. 5(b), respectively. The synthesized HRRPs of dual-channel dechirping are shown in Fig. 5(c) and the ISAR image of the target via dual-channel dechirping is shown in Fig. 5(d).

To compare the effect of pulse compression via dual-channel dechirping with pulse compression via dual-channel CS-D, we first set the number of range bins in dual-channel CS-D to be $Q = 64$ and SNR $= 20$ dB. The recovered HRRPs of channel one and channel two after motion compensation are shown in Fig. 6(a) and Fig. 6(b), respectively. After RVPs are removed, the synthesized HRRPs via the sum of the two above HRRPs are shown in Fig. 6(c). Finally, the resolution of the lower half of the ISAR image generated via dual-channel CS-D, shown in Fig. 6(d), is enhanced compared with that via dual-channel dechirping shown in Fig. 5(d).

B. DUAL-CHANNEL CS-D WITH VARIOUS RANGE BINS

The influence of the range bins of CS-D is analyzed in the following. There are 128 range bins, and the recovered HRRPs of the two channels after motion compensation are shown in Fig. 7(a) and Fig. 7(b). The synthesized HRRPs are shown in Fig. 7(c) and the ISAR image via dual-channel CS-D with 128 range bins is shown in Fig. 7(d), which is more focused than that with 64 range bins shown in Fig. 6(d).

In order to reveal the influence between the number of range bins and the resolution, more comparisons with different number of range bins ($Q = 70$, 80, and 90) are added in the simulations.

The synthesized ISAR images via dual-channel CS-D with 70, 80, and 90 range bins are shown in Fig. 8(a)–(c). Form the synthesized images, it can be seen that the

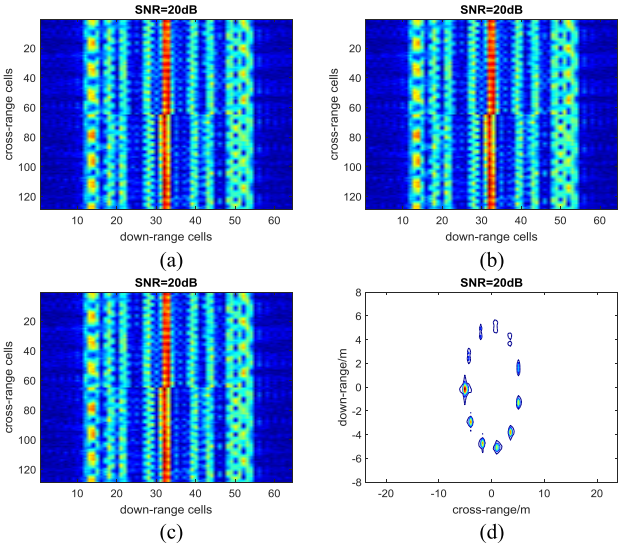

FIGURE 6. Pulse compression and ISAR imaging via dual-channel CS-D($Q = 64$). (a) HRRPs of channel 1. (b) HRRPs of channel 2. (c) Synthesized HRRPs. (d) ISAR imaging.

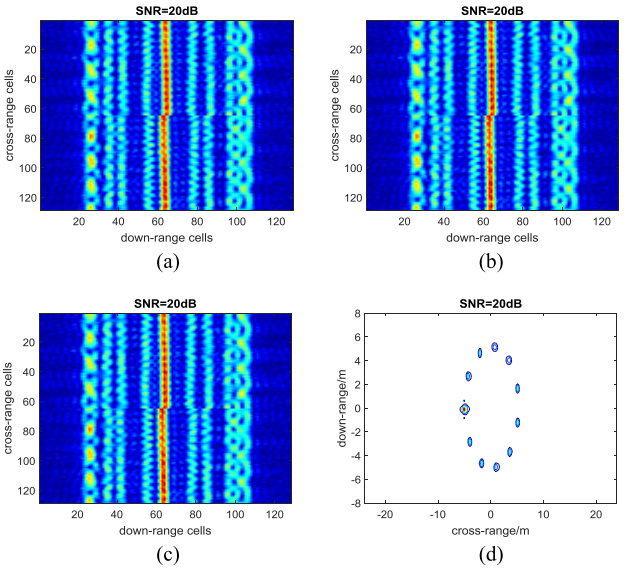

FIGURE 7. Pulse compression and ISAR imaging via dual-channel CS-D ($Q = 128$). (a) HRRPs of channel 1. (b) HRRPs of channel 2. (c) Synthesized HRRPs. (d) ISAR imaging.

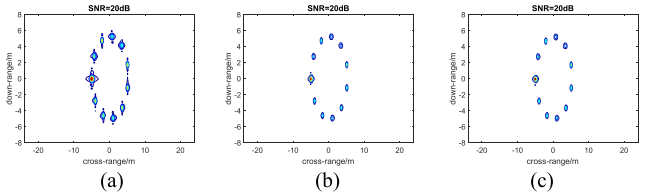

FIGURE 8. ISAR imaging via dual-channel CS-D with various Q. (a) $Q = 70$. (b) $Q = 80$. (c) $Q = 90$.

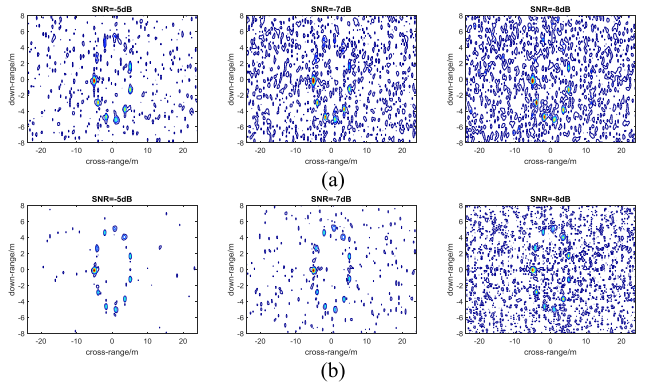

FIGURE 9. ISAR imaging via dual-channel dechirping and dual-channel CS-D under various SNRs($Q = 128$). (a) ISAR imaging via dual-channel dechirping under various SNRs. (b) ISAR imaging via dual-channel CS-D under various SNRs.

performance of pulse compression via the dual-channel CS-D improves with the number of range bins.

C. PERFORMANCE UNDER VARIOUS SNRs

To prove the robustness of the proposed dual-channel CS-D methods in a more realistic scenario, simulations with Gaussian distributed complex noise with the three SNRs of -5 dB, -7 dB and -8 dB added into the simulated V-FM signals were performed.

The ISAR imaging results via dual-channel dechirping under the three SNRs are shown in Fig. 9(a) and the ISAR imaging results via dual-channel CS-D under the three SNRs are shown in Fig. 9(b). The experiment's results show that the dual-channel CS-D can get rid of much more noise than the dual-channel dechirping method does.

D. PERFORMANCE COMPARISON WITH LFM WAVEFORMS

In order to compare the performance of V-FM waveforms with other common waveforms in radars, LFM waveforms with the same chirp rate as the above V-FM waveforms are adopted in the following simulation. The bandwidth of LFM waveforms is also set to be 300MHz and SNR $= -5$ dB. The reconstructed HRRPs of LFM waveforms via CS-D is shown in Fig. 10(a), and the reconstructed HRRPs of V-FM from channel one is shown in Fig. 10(b), the HRRPs from channel two is shown in Fig. 10(c), and the synthesized one is shown in Fig. 10(d).

From the color-bars of reconstructed HRRPs in Fig. 9, it can be seen that the SNR of the HRRPs of LFM waveforms is

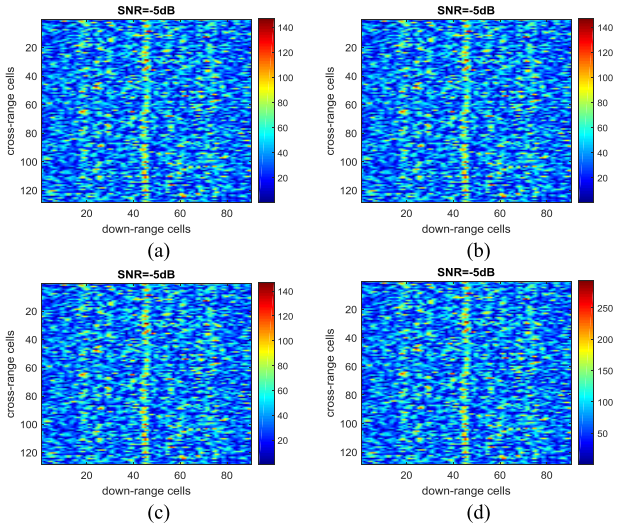

FIGURE 10. Reconstructed HRRPs of LFM Waveforms and V-FM waveforms via CS-D. (a) LFM waveforms. (b) HRRPs of V-FM waveforms (channel 1). (c) HRRPs of V-FM waveforms (channel 2). (d) Synthesized HRRPs of V-FM.

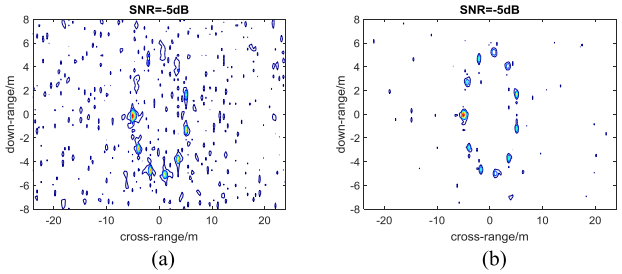

FIGURE 11. ISAR imaging of LFM Waveforms and V-FM waveforms via CS-D. (a) LFM waveforms. (b) V-FM waveforms.

similar with that of HRRPs of V-FM waveforms from channel one or two. However, the SNR of the synthesized HRRPs of V-FM waveforms is improved, which is also demonstrated by the ISAR imaging results as shown in Fig. 11(a) and Fig. 11(b).

V. CONCLUSIONS

This paper demonstrates the usefulness of the proposed dual-channel CS-D in pulse compression of V-FM waveforms. The ISAR image quality usually improves with the increment of Q, the number of range bins in dual-channel CS-D. From the analytical results, it is shown that the synthesized HRRPs and the final ISAR images via dual-channel CS-D are more robust and focused than those obtained via dual-channel dechirping under the same SNR.

ACKNOWLEDGMENT

The authors appreciate the careful and valuable comments of the anonymous reviewers to improve the quality of this paper.

REFERENCES

[1] C. Özdemir, *Inverse Synthetic Aperture Radar Imaging With MATLAB Algorithms*. Mersin, Turkey: Wiley, 2011.

[2] J. Zheng, T. Su, W. Zhu, and Q. H. Liu, "ISAR imaging of targets with complex motions based on the keystone time-chirp rate distribution," *IEEE Geosci. Remote Sens. Lett.*, vol. 11, no. 7, pp. 1275–1279, Jul. 2014.

[3] V. C. Chen and M. Martorella, *Inverse Synthetic Aperture Radar Imaging: Principles, Algorithms and Applications*. Edison, NJ, USA: SciTech Publishing, 2014.

[4] V. C. Chen and W. J. Miceli, "Simulation of ISAR imaging of moving targets," *IEE Proc.-Radar, Sonar Navigat.*, vol. 148, no. 3, pp. 160–166, Jun. 2001.

[5] A. V. Karakasiliotis, A. D. Lazarov, P. V. Frangos, G. Boultadakis, and G. Kalognomos, "Two-dimensional ISAR model and image reconstruction with stepped frequency-modulated signal," *IET Signal Process.*, vol. 2, no. 3, pp. 277–290, Sep. 2008.

[6] L. Zhang, Z.-J. Qiao, M. Xing, Y. Li, and Z. Bao, "High-resolution ISAR imaging with sparse stepped-frequency waveforms," *IEEE Trans. Geosci. Remote Sens.*, vol. 49, no. 11, pp. 4630–4651, Nov. 2011.

[7] J. Yang, X. Huang, T. Jin, J. Thompson, and Z. Zhou, "Synthetic aperture radar imaging using stepped frequency waveform," *IEEE Trans. Geosci. Remote Sens.*, vol. 50, no. 5, pp. 2026–2036, May 2012.

[8] J. Hu, J. Zhang, Q. Zhai, R. Zhan, and D. Lu, "ISAR imaging using a new stepped-frequency signal format," *IEEE Trans. Geosci. Remote Sens.*, vol. 52, no. 7, pp. 4291–4305, Jul. 2014.

[9] W. Zhou, C. M. Yeh, K. Jin, J. Yang, and Y. B. Lu, "ISAR imaging based on the wideband hyperbolic frequency-modulation waveform," *Sensors*, vol. 15, no. 9, pp. 23188–23204, 2015.

[10] W. J. Caputi, "Stretch: A time-transformation technique," *IEEE Trans. Aerosp. Electron. Syst.*, vol. AES-7, no. 2, pp. 269–278, Mar. 1971.

[11] J.-M. Muñoz-Ferreras and R. A. Gómez-García, "A deramping-based multiband radar sensor concept with enhanced ISAR capabilities," *IEEE Sensors J.*, vol. 13, no. 9, pp. 3361–3368, Sep. 2013.

[12] A. Freedman and N. Levanon, "Staggered costas signals," *IEEE Trans. Aerosp. Electron. Syst.*, vol. AES-22, no. 6, pp. 695–702, Nov. 1986.

[13] D. L. Donoho, "Compressed sensing," *IEEE Trans. Inf. Theory*, vol. 52, no. 4, pp. 1289–1306, Apr. 2006.

[14] J. A. Tropp and A. C. Gilbert, "Signal recovery from random measurements via orthogonal matching pursuit," *IEEE Trans. Inf. Theory*, vol. 53, no. 12, pp. 4655–4666, Dec. 2007.

[15] E. J. Candès and M. B. Wakin, "An introduction to compressive sampling," *IEEE Signal Process. Mag.*, vol. 25, no. 2, pp. 21–30, Mar. 2008.

[16] M. F. Duarte *et al.*, "Single-pixel imaging via compressive sampling," *IEEE Signal Process. Mag.*, vol. 25, no. 2, pp. 3–91, Mar. 2008.

[17] L. Zhang *et al.*, "Resolution enhancement for inversed synthetic aperture radar imaging under low SNR via improved compressive sensing," *IEEE Trans. Geosci. Remote Sens.*, vol. 48, no. 10, pp. 3824–3838, Oct. 2010.

[18] X. X. Zhu and R. Bamler, "Tomographic SAR Inversion by L_1-norm regularization—The compressive sensing approach," *IEEE Trans. Geosci. Remote Sens.*, vol. 48, no. 10, pp. 3839–3846, Oct. 2010.

[19] L. Zhang, Z.-J. Qiao, M.-D. Xing, J.-L. Sheng, R. Guo, and Z. Bao, "High-resolution ISAR imaging by exploiting sparse apertures," *IEEE Trans. Antennas Propag.*, vol. 60, no. 2, pp. 997–1008, Feb. 2012.

[20] X. Zhang, T. Bai, H. Meng, and J. Chen, "Compressive sensing-based ISAR imaging via the combination of the sparsity and nonlocal total variation," *IEEE Geosci. Remote Sens. Lett.*, vol. 11, no. 5, pp. 990–994, May 2014.

ZHAOYU GU received the B.S. and M.S. degrees in information and communication engineering from the National University of Defense Technology, Changsha, China, in 2006 and 2010, respectively. He is currently a Lecturer with the National University of Defense Technology. His fields of interest include radar system, radar signal processing, and FPGA programming, inverse synthetic aperture radar imaging, feature extraction, and electromagnetic environment effects.

JIAQI LIU was born in Hunan, China, in 1963. He received the Ph.D. degree in circuit and systems from Beihang University, Beijing, China, in 2007. He currently serves as the Vice Director and the Leading Research Fellow with the National Key Laboratory of Science and Technology on Test Physics and Numerical Mathematics. His research area is signal processing and target recognition.

XIAO-YI PAN was born in Anhui Province, China, in 1986. He received the M.S. and Ph.D. degrees in information and communication engineering from the National University of Defense Technology, Changsha, China, in 2009 and 2014, respectively. He is currently a Lecturer with the National University of Defense Technology. His fields of interest include inverse synthetic aperture radar imaging, feature extraction, and electromagnetic environment effects.

XIA AI was born in Yulin, China, in 1986. He received the Ph.D. degree in electromagnetics and microwave technology from Xidian University, Xi'an, China, in 2013. He currently serves as a Senior Engineer with the National Key Laboratory of Science and Technology on Test Physics and Numerical Mathematics. His research interests include computational electromagnetics, radar target recognition, and electromagnetic scattering characteristic of complex medium.

BENYUAN LIU was born in China, in 1985. He received the M.S. and Ph.D. degrees from the Science and Technology on Automatic Target Recognition Laboratory, National University of Defense Technology, Changsha, China, in 2009 and 2015, respectively. He is currently a Lecture with the Department of Bio-medical Engineering, Fourth Military Medical University. His interests lie broadly on electrical 30 impedance tomography, inverse problems, and adaptive waveform optimization.

GUOYU WANG received the Ph.D. degree in information and communication engineering from the National University of Defense Technology, Changsha, China, in 1999. He is currently a Professor with the National University of Defense Technology. His fields of interest include radar signal processing, radar system simulation, and electromagnetic environment effects.